Global coupling in excitable media provides a simplified description of mechanoelectrical feedback in cardiac tissue

E. Alvarez-Lacalle and B. Echebarria
Departament de Física Aplicada, Universitat Politècnica de Catalunya, Av. Dr. Marañón 44-50, E-08028 Barcelona, Spain
(Received 8 July 2008; revised manuscript received 16 February 2009; published 30 March 2009)

Cardiac mechanoelectric feedback can play an important role in different heart pathologies. In this paper, we show that mechanoelectric models which describe both the electric propagation and the mechanic contraction of cardiac tissue naturally lead to close systems of equations with global coupling among the variables. This point is exemplified using the Nash-Panfilov model, which reduces to a FitzHugh-Nagumo-type equation with global coupling in the linear elastic regime. We explain the appearance of self-oscillatory regimes in terms of the system nullclines and describe the different dynamical attractors. Finally, we study their basin of attraction in terms of the system size and the strength of the stretch-induced currents.

DOI: 10.1103/PhysRevE.79.031921 PACS number(s): 87.19.Hh, 05.45.−a, 87.19.R−, 89.75.−k

I. INTRODUCTION

Cardiac arrhythmias are associated with problems in the propagation of the cellular transmembrane potential, leading to the formation and, eventually, destabilization of rotors (spiral or scroll waves) [1]. To study this transition, mechanical contraction is usually neglected, being considered to be a passive consequence of electrical activity. However, simulations of simplified models of excitation-contraction coupling [2], as well as of reaction-diffusion equations in a medium with a varying (oscillatory) metric [3], suggest that mechanical deformation could play an important role on the stability of spiral waves. In cardiac muscle, besides excitation-contraction coupling, where electrophysiological changes initiate mechanical contraction in the heart, there is a feedback system whereby mechanical deformations (e.g., stretch) can modulate electric activity [4]. This is called mechanoelectric feedback (MEF) and is mediated by stretch-activated channels (SACs) in the cellular membrane [5]. The observation that atrial fibrillation is often associated with dilated atria opens the possibility that MEF plays a relevant role in the development of that arrhythmia [6,7].

The particulars of the interplay between excitation and contraction are very complex, involving the dynamics of transmembrane potential, ionic currents, intracellular calcium concentration, stretching-induced currents, and fibers strain and stress [8]. The depolarization of the cell membrane induces an increase in the intracellular calcium concentration, triggering the contraction of the cell through the development of an active tension. This active tension acts on passive tissue which has nonlinear stress-strain responses. The detailed description of these mechanisms (plus stretching-induced currents) naturally leads to complicated models which are difficult to analyze theoretically and require heavy computation time [9]. To gain insight into the possible proarrhythmic effects of mechanoelectric feedback, an alternative approach is to consider, and analyze in detail, simple models which contain the basic dynamical ingredients of MEF. With this aim, Nash and Panfilov [10] recently introduced a reduced mechanoelectrical model that considers just two variables for electrical activation and couples active stress directly to transmembrane potential. Despite its simplicity, this model presents very interesting behavior, as contraction induced oscillatory behavior [11] or instability of spiral waves [2].

The aim of this paper is twofold. First, to demonstrate that mechanoelectric coupling can lead to rather simple global feedback provided that deformations are small. It is clear that mechanoelectric feedback generates nonlocal coupling, for example, in the form of Green's functions which arise from the solution of the elastic equations with a particular set of boundary conditions. We will show that, in the linear elastic regime, elastic coupling can introduce a global feedback term where only average values of the active tension affect the local evolution of the voltage. This sets the effect of mechanoelectrical feedback in cardiac tissue in direct relation with pattern formation structures in other reaction-diffusion systems, such as the Belousov-Zhabotinsky (BZ) reaction [12], or catalytic reaction [13], such as CO oxidation on platinum [14], where the effect of global coupling in the dynamics of spirals has been studied in detail [15]. We demonstrate this relation using the one-dimensional (1D) Nash-Panfilov equations as an example of a model which, in the linear elastic limit, leads to a two-variable excitable system with global coupling. This two-variable reaction diffusion with global-coupling (RDGC) model is the most simple way to incorporate electromechanic dynamics in the heart. Models with more complex depolarization and intracellular calcium dynamics would lead to a similar simple coupling, but now with more than two variables involved.

The second aim of this paper is to show the relevance of the RDGC model in understanding cardiac-tissue dynamics. We focus on an important property of the Nash-Panfilov model. In a wide range of parameters, the dynamics of the model presents successive self-sustained pulses after an initial excitation [11]. We will show that the RDGC model reproduces all the basic properties of the Nash-Panfilov model, including this oscillatory regime. The global coupling of the RDGC model is sufficient to understand the mechanism behind the generation of these successive ectopic beats. The demonstration of this equivalence and the explanation of the mechanism behind the oscillations are made in terms of the system nullclines. We compute both the nullclines of the full Nash-Panfilov model in the case of large tissue deformations,

roughly 20%, and those of the RDGC model. In this latter case, they can be obtained semianalytically while the former requires a fully numerical approach. We will show that both nullclines are identical and present the same basic structure. This leads to a common mechanism for the explanation of the sustained oscillations.

Finally, the relevance of the model becomes more evident when we study the parameter space where oscillatory solutions are present. This analysis is possible, thanks to the numerical simplicity of the RDGC model which allows for a fast computation of the dynamics with a large number of different initial parameters. The exploration of the parameter space, together with the nullcline analysis, shows the important effect of the system length in the dynamics. It also gives approximate values for the level of stretch dependent current required to obtain oscillations. Following the same approach, we also address the long term instability of the oscillatory regime under different parameter conditions. This comprehensive analysis allows us to fully understand the details of the mechanism behind such interesting phenomena.

The outline of the paper is as follows. In Sec. I we present the Nash-Panfilov model and discuss its validity for 1D preparations of cardiac tissue, including the different contributions of active and passive stresses. Section II discusses the reduction in the Nash-Panfilov model to the RDGC model in the limit of small deformations. We discuss the validity of the reduction for an arbitrary complex model of 1D cardiac tissue. Section III is devoted to describe the oscillatory regime and study its origin using both the full Nash-Panfilov model and the RDGC model. We demonstrate that the origin of the oscillations is the same for small and large deformations via the nullcline analysis of the system. Finally, we use the RDGC model to study the parameter space where the oscillatory regime is present.

II. NASH-PANFILOV MODEL

A. Generalities

Our starting point is the Nash-Panfilov model for the transmembrane potential propagation with electromechanic feedback,

$$\partial_t V = D\nabla^2 V - \kappa_h V(V-1)(V-a) - hV - I_g, \tag{1}$$

$$\partial_t h = \epsilon(V)(\kappa_h V - h), \tag{2}$$

$$\partial_t T_a = \epsilon(V)(\kappa_T V - T_a), \tag{3}$$

$$\partial_{X_M}(S^{MN}) = 0. \tag{4}$$

Here V is the normalized dimensionless transmembrane potential, h is a recovery gate, D is the diffusion constant, X_i are the fixed reference coordinates, x_i are the material coordinates, the Laplacian operator reads $\nabla^2 V = \partial_{X_M}(\sqrt{C}C^{-1}_{MN}\partial_{X_N}V)$, S^{MN} is the first Piola-Kirchoff stress tensor, and $C_{MN}=(\partial x_k/\partial X_M)(\partial x_k/\partial X_N)$ is the right Cauchy-Green deformation tensor. The mechanical feedback is provided by a stretch-activated current

$$I_g = g(V-1)(\sqrt{C}-1)\Theta(C-1), \tag{5}$$

which only exists when the cell locally stretches, with $C=\det(\mathbf{C})$ and $\Theta(x)$ as the Heaviside function.

To obtain C a set of equations is needed relating the voltage with the contraction of the medium. The internal tension generated in the cell T_a is assumed to depend directly on the transmembrane potential V [Eq. (3)], with a delay fixed by $\epsilon(V)$, given by $\epsilon(V)=\epsilon_a$ for $V>a$ and $\epsilon(V)=\epsilon_b$ for $V<a$. The calcium dynamics and its binding to troponin C, which lead to the generation of active force in the sarcomere [8], are reduced to a simple active stress generated with a certain delay from the voltage depolarization. Finally, an isotropic hyperelastic model typical of the Mooney-Rivlin materials is introduced to describe the mechanical properties of the tissue. The first Piola-Kirchoff stress tensor is $S^{MN} \equiv T^{MN}\partial x_j/\partial X_N$, where the second Piola-Kirchhoff tensor $\mathbf{T} \equiv T^{MN}$ (total material stress) is the sum of an active $\mathbf{T}_A$ and a passive component $\mathbf{T}_W$,

$$T^{MN} = T^{MN}_W + T^{MN}_A = \left(\frac{\partial W}{\partial C_{MN}} + \frac{\partial W}{\partial C_{NM}}\right) + T_a C^{-1}_{MN}. \tag{6}$$

The strain energy function is given by

$$W = c_1(I_1 - 3) + c_2(I_2 - 3), \tag{7}$$

with $I_1=\mathrm{tr}(\mathbf{C})$ and $I_2=[(\mathrm{tr}\ \mathbf{C})^2-\mathrm{tr}(\mathbf{C}^2)]/2$ as the first and second invariants of $\mathbf{C}$. This model specifies the mechanical properties of the fiber relating the active stress T_a in the medium, its passive properties, and the displacements generated in the fiber given by $\mathbf{C}$.

The Nash-Panfilov model is a good example of a simple model which includes all the key ingredients of cardiac tissue. It presents voltage propagation, calcium-active tension dynamics, and elasticity with a mechanoelectric feedback. The electric part has the minimum number of variables necessary to obtain wave propagation using a reaction-diffusion model. More complete electric models of cardiac tissue are usually very complex, with multiple currents, gates, and ion concentrations involved [16,17]. The generation of the active tension from the raise in the voltage is a rather strong simplification of the intracellular calcium dynamics, but it incorporates the basic delay between the initial fast inward currents and the final actin-myosin contraction.

However, given that two-dimensional (2D) and three-dimensional (3D) samples of cardiac tissues are anisotropic and the Nash-Panfilov model is isotropic, this model fails to describe properly the most basic elastic behavior unless we restrict ourselves to study a one-dimensional cardiac fiber. In this latter case the hyperelastic model used by Nash-Pafilov [10] can be a correct first approximation. We think it is worth to detail when this approximation is correct. We proceed to discuss under which conditions a 3D cardiac tissue basically behaves as a hyperelastic 1D system.

B. Experimental validity of 1D hyperelastic models

In 3D systems, the basic deformation information comes from the deformation gradient $\mathbf{F}=\partial x_k/\partial X_M$ and the right Cauchy-Green deformation tensor $\mathbf{C}$ introduced in Sec. II A.

For a patch of cardiac tissue where only one dimension is relevant, the deformation can be written as

$$\mathbf{F}=\begin{pmatrix} F(X) & 0 & 0 \\ 0 & 1 & 0 \\ 0 & 0 & 1 \end{pmatrix}, \quad \mathbf{C}=\begin{pmatrix} F^2(X) & 0 & 0 \\ 0 & 1 & 0 \\ 0 & 0 & 1 \end{pmatrix}. \tag{8}$$

This structure assumes that there is no external or internally generated force which depends on coordinates y or z and that the borders of the 3D object are held fixed in the Y and Z directions in such a way that there is no friction generated at the border.

Nevertheless, it is worth remembering that there are other experimental settings which would lead to a similar deformation matrix. If the tissue is very thin in the Z direction, the plane stress approximation can be carried out for the plane X-Y. The error introduced by considering Eq. (8) would be of order b^2 (with b being the thickness of the tissue). In this situation, the starting point is generally a 2×2 matrix where the third rows and columns of $\mathbf{F}$ and $\mathbf{C}$ are eliminated.

Furthermore, under general assumptions, provided that the scale of the remaining dimension of the system is much larger than the other, normal tensions at the extreme will have very small effects away from the edges. So, one can imagine an experimental situation of a very thin cubic tissue with in-plane fibers pointing in the X direction while having a large Y dimension compared with the length of the fibers. The 1D solution obtained for $F(X)$ would be the leading contribution of the exact solution for the strain field.

In summary, the 1D approximation is experimentally relevant under some specific conditions. Let us now explain in more detail how the passive and active stresses appear under the Nash-Panfilov formulation and use it to reduce the complex elastic equations from three dimensions to one dimension.

C. 1D elastic equation

To obtain the 1D equation for the Mooney-Rivlin model, we first use the energy indicated in Eq. (7). The second Piola-Kirchhoff (material) stress $\mathbf{T}_W$ related with the elastic energy is obtained by performing the formal derivatives $\partial W/\partial C_{MN}$ indicated in Eq. (6) (see [18] for more details), so

$$\mathbf{T}_W=2[c_1+c_2\,\mathrm{tr}(\mathbf{C})]\mathbf{I}-2c_2\mathbf{C}. \tag{9}$$

Considering Eq. (8) and 3×3 matrices (we take $D=3$ here but keep the possibility of $D=2$ open), the first Piola-Kirchhoff (nominal) stress $\mathbf{S}_W=\mathbf{T}_W\cdot\mathbf{F}^T$ reads [18]

$$\mathbf{S}_W=2(c_1+2c_2)\begin{bmatrix} F(X) & 0 & 0 \\ 0 & 1 & 0 \\ 0 & 0 & 1 \end{bmatrix}+2c_2[F^2(X)-1]\begin{pmatrix} 0 & 0 & 0 \\ 0 & 1 & 0 \\ 0 & 0 & 1 \end{pmatrix}. \tag{10}$$

Notice that in this model, $\mathbf{S}_W$ has an isotropic component which is not zero in the absence of external forces. To bring the system close to its natural state one needs an internal constant isotropic pressure $\mathbf{p}=p\mathbf{I}$. There are two different direct ways to implement this pressure, as a constant pressure in the real configuration (Cauchy stress tensor) or as an isotropic pressure in the reference configuration following the same structure as the active stress $\mathbf{T}_A=T_a(X)\mathbf{C}^{-1}$. The difference between both is a factor including the determinant of the deformation gradient.

We consider the first approach so that the passive tensor $\mathbf{S}_{pas}$ reads

$$\mathbf{S}_{pas}=\mathbf{S}_W+p\,\det(F)\mathbf{F}^{-1}. \tag{11}$$

The pressure p can now be obtained by requiring $\mathbf{S}_{pas}=0$ when $F(X)=1$. This leads to $p=-\tilde{c}$, where $\tilde{c}=2[c_1+(D-1)c_2]$ is generalized for any dimension.

The full tensor $\mathbf{S}=\mathbf{T}\cdot\mathbf{F}^{\mathbf{T}}$ with active and passive parts now becomes

$$\mathbf{S}=\mathbf{S}_W-\tilde{c}\,\det(F)\mathbf{F}^{-1}+T_a\mathbf{C}^{-1}\cdot\mathbf{F}^{\mathrm{T}}. \tag{12}$$

Now, we apply the conservation of momentum [Eq. (4)] to get

$$\partial_X\left[S_W^{11}+p+\frac{T_a(X)}{F(X)}\right]=\partial_X\left[\tilde{c}[F(X)-1]+\frac{T_a(X)}{F(X)}\right]=0, \tag{13}$$

where the other components of the momentum conservation are fulfilled by construction. Therefore, in the X direction the total stress is a constant,

$$\tilde{c}[F(X)-1]+\frac{T_a(X)}{F(X)}=B. \tag{14}$$

Passive stress is related with the deformation via $S_{pas}^{11}=\tilde{c}u$, being $u=F-1$, while the active stress is related with $T_a/(1+u)$.

Notice that in the formulation of Eq. (4), the constant pressure can be omitted and the momentum conservation written as

$$\partial_X(TF)=0, \quad \text{with} \quad T(X)=\tilde{c}+T_a(X)/F^2(X). \tag{15}$$

Finally, the stretch current formulated in Eq. (5) can be written in terms of $F(X)$ as

$$I_g=g(V-1)(F-1)\Theta(F-1). \tag{16}$$

To conclude this section, let us sum up the Nash-Panfilov model in one dimension. The model is defined by Eqs. (1)–(3), (15), and (16). In particular, from now on, we will consider the plane stress approximation ($D=2$) and define $\tilde{c}=2(c_1+c_2)$.

III. ELASTIC APPROXIMATION AND RDGC MODEL

As discussed in Sec. I, we will show not only that the mechanoelectric feedback can generate global couplings but that this coupling is sufficient to understand the mechanism behind the oscillatory regime in the Nash-Panfilov model [10] discussed in Ref. [11].

To this aim, we perform now the small deformation approximation of the 1D Nash-Panfilov model. The result will be a two-variable model with global coupling which becomes the first-order elastic approximation for any kind of

hyperelastic model considered. Indeed, we will proof in this section that other initial models would lead naturally to the same kind of model with global coupling.

A. Small deformation limit

Let us start with the small deformation approximation, which we can write as $F \simeq 1+u(X)$, with $u \ll 1$. Then, Eq. (15) can be integrated to

$$\tilde{c}[1+u(X)] + T_a(X)[1-u(X)] = A. \tag{17}$$

The deformation gradient becomes $F(X) \simeq 1+u(X) = [A-T_a(X)]/\tilde{c}$ when $T_a \ll \tilde{c}$. The integration constant A is determined by the boundary conditions. If we fix the external tension of the fiber at T_e we can use Eq. (14) to obtain $A = \tilde{c}+T_e$ and $F(X)=1+[T_e-T_a(X)]/\tilde{c}$. In the more interesting case where the fiber is fixed at the extremes $[x(0)=0,\ x(L)=L]$, then

$$\int_0^L F(X)dX = L, \tag{18}$$

so $A=\tilde{c}+\bar{T}_a$, with $\bar{T}_a$ being the average value of T_a along the line. The deformation gradient becomes

$$F(X) = 1 + [\bar{T}_a - T_a(X)]/\tilde{c}, \quad \text{with } \bar{T}_a = \frac{1}{L}\int_0^L T_a(X)dX. \tag{19}$$

Thus, the stretching is directly related to the active tension. If, at a given location, the active tension is lower (higher) than the average active tension in the system, then the fiber experiments an extension (contraction) at that point. In this way we can write Eqs. (1)–(3) and I_g as a closed system of equations. Particularly,

$$I_g = (g/\tilde{c})(V-1)(\bar{T}_a - T_a)\Theta(\bar{T}_a - T_a). \tag{20}$$

It is worth mentioning that the condition $T_a \ll \tilde{c}$ in the paper does not imply that passive stresses are much smaller than active stresses. In fact, both in the case of small and large deformation active stress is at least twice the passive stress.

B. RDGC model

The Nash-Panfilov model can be further simplified because T_a and h are directly related by $T_a=(\kappa_T/\kappa_h)h$ given that $\epsilon(V)$ is the same in both cases. By considering $g \sim 1/u$ we can write the equivalent system at zeroth order as

$$\partial_t V = D\partial_X^2 V - \kappa_h V(V-1)(V-a) - hV - G(V-1)(\bar{h}-h)\Theta(\bar{h}-h), \tag{21}$$

$$\partial_t h = \epsilon(V)(\kappa_h V - h), \tag{22}$$

where $\bar{h}$ is the instantaneous average value of h in the whole tissue giving rise to the global coupling I_g and $G=(g/\tilde{c})(\kappa_T/\kappa_h)$ is the key constant which encompasses the conductance of the channel g, the elastic properties of medium $\tilde{c}$, and the ratio of activation times κ_T/κ_h.

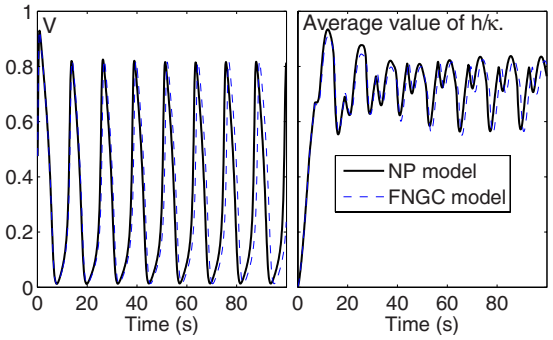

FIG. 1. (Color online) Using the parameters employed in [11] we show that the full Nash-Panfilov model (solid line) and the approximate linear model (dashed line) are equivalent. Left panel: voltage at the center of the line as a function of time. Right panel: average value of h/κ_h along the line. Parameters of the Nash-Panfilov model: $L=6$ cm, $D=1$ mm^2/s, $\kappa_h=8$ s^{-1}, $a=0.05$, $\epsilon_a=0.1$ s^{-1}, $\epsilon_b=1.0$ s^{-1}, $k_T=5$ MPa, $\tilde{c}=16$ MPa, and $g=1.6$ s^{-1}.

Up to a maximum elongation of around 10% Eqs. (1)–(3), (15), and (16), on one hand, and Eqs. (21) and (22), on the other, are equivalent. Figure 1 presents an example of how both models reproduce the same results for a case with maximum elongation of around 5% $\{\max[u(X)]=0.05\}$. We observe that the main difference between both simulations arises from differences in the frequency of the oscillatory regime. It is worth stressing that these small differences in frequency accumulate eventually leading to a shift in time between the exact and small deformation solution. Therefore, comparing the state of the system in both situations after a long time will not produce comparable results.

However, the type of behavior and the dynamics within one cycle is almost exact. This point is checked in Fig. 2 where we plot in the bottom graph the instantaneous value of the voltage along the line. Once the voltage profile is given, the exact instantaneous deformation $u(X)$ found solving the full nonlinear Nash-Panfilov problem is the same as the linear approximation of the deformation obtained from Eq. (19).

C. Generality of the minimal model

The same general small deformation limit used to obtain the RDGC model can be applied to more general electric models where voltage is controlled by multiple gates and ion concentrations $\vec{h}=(h_1,h_2,\ldots)$. Equally, models with more detailed calcium-troponin C-tropomyosin dynamics have higher number of equations which lead to a more complex generation of T_a. In both cases, however, the basic mechano-electric feedback would remain unchanged. Generally, the MEF mechanism in the elastic regime would appear as a stretch-induced current which has the functional dependence $I_g(V,\vec{h},T_a,\bar{T}_a)$, with $\bar{T}_a$ providing the global coupling.

It is important to stress that this general outline does not necessarily follow when we consider more complex elastic models. A general elastic model can be highly complex, including cases where the total stress cannot be written simply

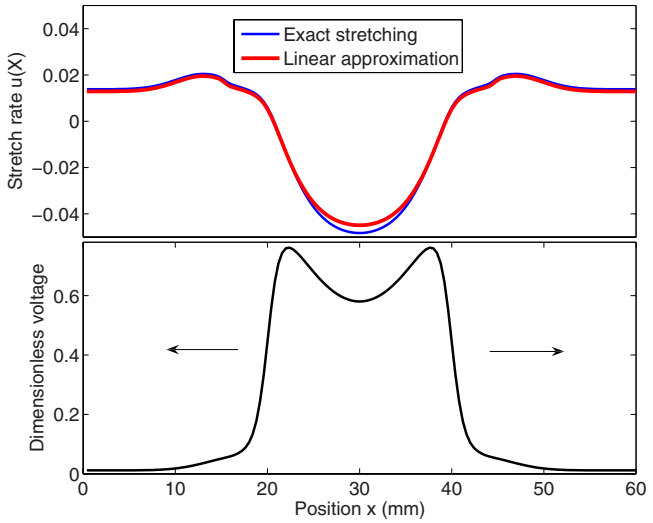

FIG. 2. (Color online) Bottom panel: instantaneous shape of the voltage as a function of distance after an initial external activation at the center of the line. The final state is a series of periodic pulses originated at the center which propagate in both the left and right directions. The model used to describe the evolution is the full Nash-Panfilov model with parameters $L=6$ cm, $D=1$ mm^2/s, $\kappa_h=8$ s^{-1}, $a=0.05$, $\epsilon_a=0.1$ s^{-1}, $\epsilon_b=1.0$ s^{-1}, $k_T=5$ MPa, $\tilde{c}=16$ MPa, and $g=1.6$ s^{-1}. Top panel: in black (blue) the exact instantaneous deformation $u(X)$ corresponding to the state indicated in the bottom panel. The exact solution is found solving the full nonlinear Nash-Panfilov problem obtaining $F(X)$ and then using $u(X)=F(X)-1$. This solution is compared with the linear approximation of the deformation—gray (red) line—obtained from Eq. (8) in the paper, which gives $u(X)=[\bar{T}_a-T_a(X)]/\tilde{c}$. This gives an idea of the error we make when we substitute the full elastic equations by their linearized version.

as the sum of a passive and active part. Then, the first-order approximation of small deformations could be different from the one we find here. In general, however, a realistic model of the heart can be written as having a passive component with a deformation limit plus an active tension generated by the calcium intake. Far from the deformation limit, the passive stresses can be properly approximated by a nonlinear hyperelastic model. We have included in the Appendix a detailed description of how a general 1D nonlinear hyperelastic model is reduced in the appropriate limit to our small deformation model. The reduction is useful because it allows us to show that the differences between a general hyperelastic material and the passive elastic approximation used in the Nash-Panfilov equation are small.

This allows us to state that the RDGC model is a good approximation for any hyperelastic material considered as a model of cardiac tissue in one dimension. This statement has an important caveat. The largest contribution of the active stress tensor should have the same structure as in the Nash-Panfilov model. This means that it must be added to the passive part, as mentioned, and it must behave as $T_a(X)$ as $F\approx 1$.

Finally, we do not address here the generality of the model for 2D and 3D systems. Boundary conditions in higher dimensional system could lead to different types of

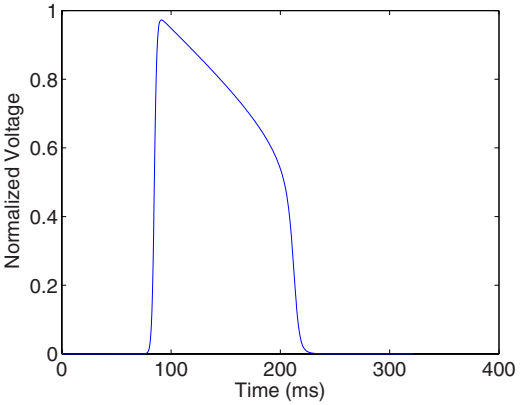

FIG. 3. (Color online) Typical shape of the action potential corresponding to a pulse initiated at one end of the line and measured at 5 cm from the end. Parameters are $L=10$ cm, $D=1$ cm^2/s, $\kappa_h=2000$ s^{-1}, $a=0.05$, $\epsilon_a=3$ s^{-1}, and $\epsilon_b=90$ s^{-1} with no stretching $G=0$.

nonlocal couplings. In particular, highly nonlocal couplings via the propagation of the solution in the form of Green's functions must be present in 3D system with changing boundary conditions (such as in the heart). Thus, whether this simple global coupling is an accurate and useful first-order approximation of the nonlocal coupling generated by the elastic equations in higher dimensional anisotropic systems remains an open question. Let us mention, however, that we have proven that this is indeed the case for 2D radially symmetric models [19].

IV. GLOBAL COUPLING AS THE ORIGIN OF THE CONTINUOUS GENERATION OF ECTOPIC BEATS

The Nash-Panfilov model presents a broad range of parameters for which the system shows an oscillatory regime with the successive generation of self-sustained pulses after an initial excitation [11]. We address now the origin of this behavior and show that the global coupling present in the RDGC model is sufficient to understand the mechanism behind the generation of these ectopic beats. We prove this point by comparing the nullclines of the full model—having tissue deformations of ~20%—with the nullclines of the RDGC model.

A. Description of the oscillatory regime

Let us begin showing that the simplified model also presents the characteristic oscillatory behavior of the full Nash-Panfilov model. In the present and following sections of the paper we will take $D=1$ cm^2/s, $\kappa_h=2000$ s^{-1}, $a=0.05$, and $\epsilon_a=3$ s^{-1}, which give reasonable values of the action potential duration [(APD)$\simeq$125 ms] and conduction velocity [(CV)$\simeq$30 cm/s] in the absence of stretching-induced current. Figure 3 presents a characteristic action potential generated by the simple Nash-Panfilov electric model using these parameters

In these conditions, the length of the system L, the normalized strength of the stretching-induced current G, and ϵ_b

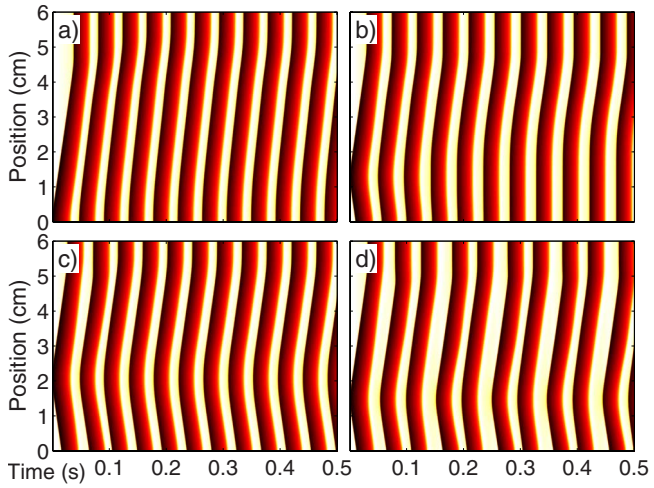

FIG. 4. (Color online) Four different attractors in the oscillatory regime for $L=6$ cm, $\epsilon_b=90$ s^{-1}, and $G=0.04$ [except for graph (d) where $G=0.035$] (see text for more details).

set us in a three-parameter space which, together with the initial condition, defines completely the dynamics of the line. Modifying these parameters, we have systematically found four characteristic kinds of stable oscillatory attractors shown in Fig. 4. In Fig. 4(a) the initial excitation is given at one end of the cable, while in Figs. 4(b)–4(d) it is started at an arbitrary point of the line. The most typical patterns are oscillations with a source at a position that depends on the initial condition [Figs. 4(a) and 4(c)]. The other two characteristic oscillations include a final state where two regions of tissue depolarize alternatively [Fig. 4(b)] and, in very special cases, a final state where the time between two consecutive pulses alternates, as shown in Fig. 4(d).

B. Nullcline analysis of the oscillatory regime in the Nash-Panfilov and in the minimal model

To explain this behavior we must understand the mechanism that generates the oscillatory regime. For that, it is helpful to study the nullclines of the RDGC model. From Eqs. (21) and (22) we find that one of the nullclines is just $h=k_hV$, while the other reads

$$h = -\kappa_h(V-1)(V-a), \quad \text{if } h > \bar{h}, \tag{23}$$

$$h = \frac{V-1}{V-G(V-1)}[-\kappa_h V(V-a) - G\bar{h}], \quad \text{if } h < \bar{h}. \tag{24}$$

Notice that $\bar{h}$ changes with the evolution of $h(X,t)$ and must be computed numerically at each time step from the two-variable model.

We address now whether this approach provides a faithful qualitative picture by computing the nullclines of the full model. In this latter case, the first nullcline $h=k_hV$ does not change, but the second nullcline is now more difficult to obtain since we do not have an analytical expression for $I_g(h)$. We need first the deformation F expressed numerically

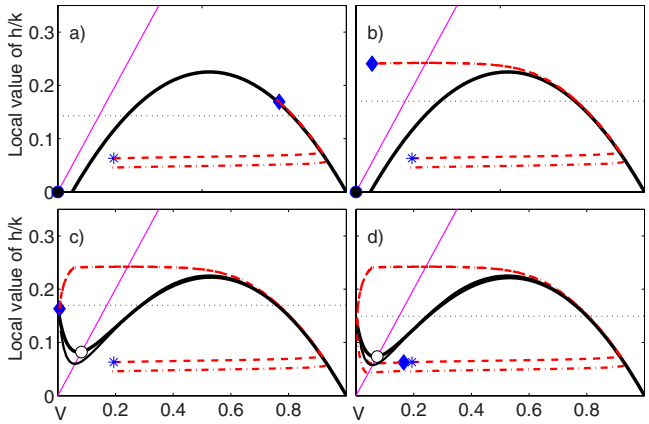

FIG. 5. (Color online) Four snapshots of the nullclines and the phase space (V,h) evolution at the end of the line where waves are generated. Gray (magenta) thin solid curve corresponds to $h_t=0$. Black thicker curve shows $V_t=0$ for small deformations, and black thinner curve shows $V_t=0$ computed numerically according to Eqs. (26) and (27). The trajectories (V,h) at $x=0$ in phase space are indicated by the gray (red) dotted-dashed line for large deformations and gray (red) dashed line for small deformations. For the case of small deformation, the black dotted line indicates the instantaneous value of $\bar{h}/\kappa_h$, the initial (V,h) is represented by a star, and the instantaneous by a diamond. Black (white) circle indicates unstable (stable) fixed point.

as $F(h)$. From Eq. (15) the full nonlinear solution of F reads as

$$F(X) = \frac{\alpha}{2} + \sqrt{\left(\frac{\alpha}{2}\right)^2 - \frac{\kappa_T h(X)}{\tilde{c}\kappa_h}}, \tag{25}$$

where α is set by the boundary condition and computed numerically every time step. Notice that in the case of a fixed external tension it is not necessary to compute α numerically since we would have $\alpha=(\tilde{c}+T_e)/\tilde{c}$. In any case, $F(h)$ is obtained formally and introduced in the second nullcline equation,

$$h = -\kappa_h(V-1)(V-a), \quad \text{if } F < 1, \tag{26}$$

$$h = \frac{V-1}{V}\{-\kappa_h V(V-a) - g[F(h)-1]\}, \quad \text{if } F > 1. \tag{27}$$

Figure 5 presents a series of four snapshots of the nullclines at different times in one cycle of the oscillation. We plot both the nullclines for a small deformation case [corresponding to the simulations in Fig. 4(a) using the semianalytical expressions [Eqs. (23) and (24)] and a case with deformations up to 20% using the fully numerical nullclines obtained from Eqs. (26) and (27)]. In both cases L and ϵ_b are the same. We also track the evolution of h and V at the source of successive waves $x=0$ and plot their instantaneous values. To visualize better the process, if instantaneously $h(0)>\bar{h}$, we take the expression of the nullclines from Eq. (23) [or Eq. (26) if instantaneously $I_g(0)=0$].

Both approaches produce very similar results, demonstrating that the mechanism for the oscillation in the full model is effectively captured by our small deformation analysis. This mechanism can now be explained as follows. Once the wave has originated, the variable h increases above the average value in tissue $\bar{h}$ [Fig. 5(a)]. At this point, the stretch-activated channels close at the origin, which begins to recover [Fig. 5(b)]. In this situation, the two nullclines intersect at the stable point $V=0$, $h=0$. If the relaxation is such that $\bar{h}$ remains significantly above zero because some other part of the line is active (i.e., a wave is still propagating along the line), the nullclines suddenly change due to the opening of the stretch-activated channels [Fig. 5(c)]. Then, $V=0$ is no longer a steady state, and it is replaced by an unstable fixed point which pushes again the voltage toward depolarization [Fig. 5(d)]. This generates another wave which propagates along the line, closing the oscillation loop.

In other words, the general mechanism for the oscillation can be tracked to the global-coupling mechanism produced by the mechanoelectric feedback. Once a pulse is emitted, the variable h at the source point goes locally below the average value, and the stretch-activated channels open. If the parameters are adequate, this originates successive excitations at the same point, resulting in oscillatory behavior. This mechanism is the same both in the linear elastic regime and in the full Nash-Panfilov model.

V. ANALYSIS OF THE OSCILLATORY REGIME USING THE MINIMAL MODEL

The study of the RDGC model provides further insight on the range of parameters under which the oscillatory regime appears. Since Eqs. (21) and (22) integrate out the elastic equation in the Nash-Panfilov model, simulations are much faster and allow us to study the basin of attraction of the oscillatory regime when the initial excitation is at the end of the line. The final attractor of the dynamics is either the trivial fixed point ($V=0$ along the line), the attractor shown in Fig. 6(a), or the one in Fig. 6(b) (in this latter case, the source moves from the extreme to another point on the line).

By scanning systematically the parameter space (G,L) we observe that the appearance of oscillatory dynamics requires both a minimum value of G which increases slightly as L increases and a minimum length of the system. For small refractory time ϵ_b (see Fig. 6), a large portion of the phase space produces initially a series of waves which are not exactly periodic and die out after a long transient. As the recovery time ϵ_b increases, trajectories approach faster one of the attractors and oscillatory regimes concentrate around $L=6-7$ cm.

The nullcline analysis and the phase portrait of Fig. 6 lead to an important set of conclusions.

(i) The value of G has to be large enough so that, when the stretch-activated channels open, the nullclines intersect in the unstable branch of the cubic nullcline, generating an unstable fixed point.

(ii) A global oscillatory regime requires $\bar{h}$ to oscillate around a fix high value, otherwise the stretching-induced current would not be activated at the excitation point. The appearance of new waves at one point has to be compensated with the disappearance of waves which reach the other end of the line. This makes the length of the system and the wave speed crucial elements of the ectopic generation.

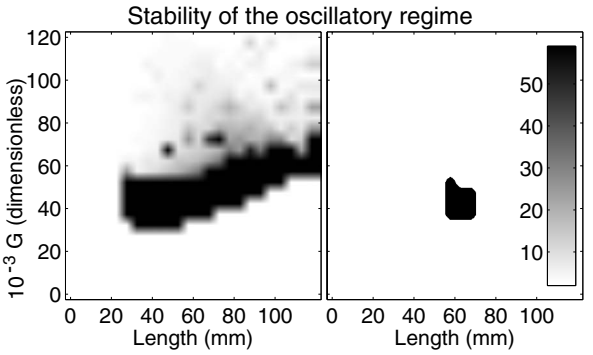

FIG. 6. Basin of attraction of the oscillatory regime with initial excitation at one end of the sample for $\epsilon_b=90$ s^{-1} (left graph) and for $\epsilon_b=30$ s^{-1} (right graph). White area indicates lack of successive waves. Black areas indicate stable oscillatory regime. Gray areas indicate initial generation of waves which eventually die out. Color bar indicates relation between gray level and time before activity die out in seconds.

(iii) Furthermore, if the system is too small or the recovery (ϵ_b) too low, no oscillation can be sustained because h has similar values along the tissue, making the difference $\bar{h}-h$ almost nil.

(iv) The stable oscillatory regime requires $\bar{h}$ to reach a perfect global periodicity. The long term oscillations which eventually die off can be understood in terms of the amplification of small perturbations in the $\bar{h}$ orbit. These small perturbations do not prevent immediately the generation of new waves, but eventually $\bar{h}$ can move away from high values and prevent the activation of I_g at the source of the waves. We present different movies describing these phenomena in [20].

We should also notice that oscillations disappear for large G. In this case, after the initial excitation at the origin, the strong I_g current activates uniformly a large segment in the opposite end of the line before the propagating wave reaches it. As a consequence, $\bar{h}$ spikes and then decreases rapidly. The resulting I_g current is too small to generate a new wave. Furthermore, the high excitability of the system amplifies small changes in $\bar{h}$ from one cycle to another (if present) impeding $\bar{h}$ to reach a global oscillation. These deviations from periodicity in $\bar{h}$ arrive from parts of the tissue that can be alternatively excited either by wave diffusion (the arrival of a pulse activates them) or by the I_g current.

VI. DISCUSSION AND CONCLUSION

We have found that a reaction-diffusion model with global coupling includes the main effect of mechanoelectric feedback under some experimental conditions. Specifically, it is the first-order approximation of any hyperelastic model of

1D cardiac tissue. It includes two variables so as to be able to generate a propagating pulse plus a global-coupling term where a spatial average of the variables is involved in the generation of the depolarization. We have described the specific experimental conditions where this model would be useful to analyze the dynamics. The most common of which would be a very thin sample of cardiac tissue with a small fixed length along the fibers. This model sets *in vitro* cardiac-tissue dynamics in direct relation with some catalytic reaction and reaction-diffusion systems where global coupling also plays a crucial role.

Particularly, we have shown the relevance of the model in describing the mechanism and the conditions under which a 1D experimental sample would present successive self-sustained ectopic beats. The mechanism behind these phenomena can be understood in terms of the stretch-induced current which enters the cell only when the local active tension is below the average value along the cell. This requires a minimum conductivity for the stretch-activated channels to sustain the oscillation, together with an adequate length of the system. Small samples would lead to an almost simultaneous depolarization along the fiber without big differences in the stretching across the sample. Samples which are too large would not only generate another pulse at the same place of the previous excitation but also in front of the propagating wave. Both cases make the generation of successive waves at the same point of the sample impossible.

A very important and difficult question remains to be answered. It relates to the generality of the global coupling presented in the RDGC model for systems with higher dimension. It is not clear from our analysis if 2D and 3D anisotropic models would have the same kind of first-order nonlocality. The standard solution of 2D and 3D anisotropic elasticity problems in the limit of small deformations depends heavily on the boundary conditions. While a particular nonlocal solution involving Green's functions could be compared with a simple average solution (for instance, in the case of radial symmetry in two dimensions; see Ref. [19]), it is not clear how this could be generalized to all particular configurations. In one dimension, a fiber with a fixed extension implies couplings related with the global average, while fixed tension at the extreme implies a local system of equations. This kind of statements could be difficult to reproduce in three dimensions given the different sets of tissue shapes and boundary conditions possible. Furthermore, it could also happen that the first-order approximation of the elastic equations is a particular form of Green's function in the same sense that in one dimension the proper first-order Green's function is the identity. In any case, given the important insights obtained in one dimension, pursuing the first-order approximation in 2D and 3D systems could be worthwhile. Especially, it could be helpful to understand the effects of elasticity on the stability of fully nonlinear spiral waves.

Concluding, we have been able to understand the underlying physical mechanism of the oscillatory regime in the Nash-Panfilov model demonstrating its equivalence to a reaction-diffusion model with global coupling and studying its nullclines. We demonstrated the generality of this coupling as a first-order approximation for any 1D cardiac-tissue model. We also obtained the basin of attraction of the oscillatory regime for initial excitations at the end of the line. Although it is known [9] that local deformations of up to 10% can produce a single stretch generated action potential, we have shown that successive and sustained generation of ectopic excitations depends crucially on the relations between the length of the system and wave speed/recovery time of the pulse. This fruitful analysis indicates that similar models with mechanoelectric coupling for 2D–3D tissue, where the anisotropy is taken into account, could be equally useful to understand anomalous cardiac behavior.

ACKNOWLEDGMENTS

We thank F. H. Fenton, E. Cherry, and J. L. Rodríguez for valuable discussions. This study was supported by MEC (Spain), under Projects No. FIS2005-06912-C02-01 and No. FIS2008-06335-C02-01, and under the Ramón y Cajal (B.E.) and Juan de la Cierva (E.A-L.) programs.

APPENDIX: GENERALITY OF THE MINIMAL MODEL

In this appendix we discuss the limit of small deformations for a general hyperelastic model. To this end, we recall that a hyperelastic 3D model has an elastic energy close to its natural state which can be expanded in terms of the displacement tensor $\mathbf{E}=(\mathbf{C}-\mathbf{I})/2$ (see, for example, [18]). This leads to a second Piola-Kirchhoff stress tensor of the form

$$\mathbf{T}_{pas}=\lambda\ \mathrm{tr}(\mathbf{E})\mathbf{I}+2\nu\mathbf{E}+O(\mathbf{E}^2). \tag{A1}$$

Now we check how this model would read when one considers a 1D system. Taking into account Eq. (8) and neglecting the higher order terms, we get

$$\mathbf{T}_{pas}=\begin{pmatrix}(\lambda+2\nu)(F^2-1)/2 & 0 & 0\\ 0 & \lambda(F^2-1)/2 & 0\\ 0 & 0 & \lambda(F^2-1)/2\end{pmatrix}. \tag{A2}$$

Adding the active part and using the conservation of momentum we obtain

$$\partial_X\left\{\frac{\lambda+2\nu}{2}[F^2(X)-1]F(X)+\frac{T_a(X)}{F(X)}\right\}=0. \tag{A3}$$

This model obviously reduces to the Rivlin-Moonley case in the limit of very small deformations with a redefinition of the constants. Comparing the relevant passive part,

$$(\lambda+2\nu)(F^2-1)/2=(\lambda+2\nu)u(X)[1+0.5u(X)][1+u(X)], \tag{A4}$$

with the expression obtained for the Rivlin-Moonley case $\tilde{c}(F-1)=\tilde{c}u$ we find that $\tilde{c}=(\lambda+2\nu)$ in the limit of small deformations.

Notice that these two models give equivalent results as long as $[1+0.5u(X)][1+u(X)]\approx 1$. Therefore, the largest term we are neglecting in this approximation would introduce corrections to our linear elastic model which go as

$1.5u(X)$. This means that for deformations of up to 10% we should obtain errors of the order of 15%. For example, 10% deformations using this model correspond to deformations up to 12% in the model we use in the paper. These differences cannot change the basic framework of global coupling when the boundaries are fixed and will not change significantly any of the results of the paper, in particular the nullcline analysis we perform in Sec. IV B.

[1] See, e.g., the focus issue on fibrillation in normal ventricular myocardium, Chaos **8** (1) (1998).

[2] A. V. Panfilov, R. H. Keldermann, and M. P. Nash, Proc. Natl. Acad. Sci. U.S.A. **104**, 7922 (2007).

[3] H. Zhang, B.-W. Li, Z.-M. Sheng, Z. Cao, and G. Hu, Europhys. Lett. **76**, 1109 (2006); H. Zhang, X. S. Ruan, B. Hu, and Q. Ouyang, Phys. Rev. E **70**, 016212 (2004).

[4] See, e.g., the special issue on mechanoelectric feedback and cardiac arrhythmias, P. Kohl and U. Ravens (editors) Prog. Biophys. Mol. Biol. **82** (2003).

[5] P. Kohl, P. Hunter, and D. Noble, Prog. Biophys. Mol. Biol. **71**, 91 (1999).

[6] M. B. Wagner, R. Kumar, R. W. Joyner, and Y. Wang, Eur. J. Physiol. **447**, 819 (2004).

[7] M. R. Franz and F. Bode, Prog. Biophys. Mol. Biol. **82**, 163 (2003); F. Ravelli, *ibid.* **82**, 137 (2003).

[8] P. J. Hunter, A. D. McCulloch, and H. E. D. J. ter Keurs, Prog. Biophys. Mol. Biol. **69**, 289 (1998).

[9] S. Hirabayashi, M. Inagaki, and T. Hisada, J. Cardiovasc. Electrophysiol. **19**, 730 (2008).

[10] M. P. Nash and A. V. Panfilov, Prog. Biophys. Mol. Biol. **85**, 501 (2004).

[11] A. V. Panfilov, R. H. Keldermann, and M. P. Nash, Phys. Rev. Lett. **95**, 258104 (2005).

[12] V. K. Vanag, L. Yang, M. Dolnik, A. M. Zhabotinsky, and I. R. Epstein, Nature (London) **406**, 389 (2000); E. Mihaliuk, T. Sakurai, F. Chirila, and K. Showalter, Phys. Rev. E **65**, 065602(R) (2002).

[13] U. Middya, D. Luss, and M. Sheintuch, J. Chem. Phys. **100**, 3568 (1994).

[14] M. Kim, M. Bertram, M. Pollmann, A. von Oertzen, A. S. Mikhailov, H. H. Rotermund, and G. Ertl, Science **292**, 1357 (2001); M. Falcke and H. Engel, J. Chem. Phys. **101**, 6255 (1994).

[15] V. S. Zykov and H. Engel, Phys. Rev. E **66**, 016206 (2002).

[16] F. B. Sachse, *Computational Cardiology: Modeling of Anatomy, Electrophysiology, and Mechanics*, Lecture Notes in Computer Science (Springer, Verlag, Berlin, 2004).

[17] A. J. Pullan, M. L. Buist, and L. K. Cheng, *Mathematically Modeling the Electrical Activity of the Heart: From Cell to Body Surface and Back* (World Scientific, Singapore, 2005).

[18] P. G. Ciarlet, *Mathematical Elasticity* (North-Holland, Amsterdam, 1993), Vol. 1.

[19] E. Alvarez-Lacalle, J. F. Rodríguez, and B. Echebarria, Comput. Cardiol. **35**, 189 (2008).

[20] See EPAPS Document No. E-PLEEE8-79-049903for movies of the evolution and corresponding nullclines for stable and unstable oscillatory dynamics. For more information on EPAPS, see http://www.aip.org/pubservs/epaps.html.